ADVANCED FUNCTIONAL MATERIALS
www.afm-journal.de

A Multifunction Heterojunction Formed Between Pentacene and a Single-Crystal Silicon Nanomembrane

Jung-Hun Seo, Tae-Yeon Oh, Jungho Park, Weidong Zhou, Byeong-Kwon Ju, and Zhenqiang Ma**

A mesh patterned n-type single-crystalline silicon nanomembrane (SiNM) created from a silicon-on-insulator (SOI) wafer is complementally combined with a p-type pentacene layer to form a heterogeneous p-n junction on a flexible plastic substrate. Excellent rectifying characteristics are obtained from the heterogeneous p-n diode. The diode also exhibits photosensitivity at visible wavelengths with a photo-to-dark current ratio exceeding four orders, a responsivity of 0.7 A/W, and an external quantum efficiency of 21.9% at 633 nm. Over 60% average transmittance in the visible spectrum is measured from the heterogeneous multilayer junction on a plastic substrate. Outstanding mechanical bending characteristics are observed with up to 1.08% of strain applied to the diode. These results suggest that organic-inorganic heterogeneous integration may be a viable strategy to build flexible organic-inorganic heterojunction devices and thus enable a number of novel multifunctional applications.

1. Introduction

In recent years, there have been many attempts to integrate inorganic and organic semiconductors to form hybrid structures in order to take the advantages of each material.[1–14] It has been shown in earlier reports that inorganic and organic hybrid combination has clear complementary advantages, such as high carrier mobility and wider absorption spectrum from the inorganic side, and low temperature solution processability and low-cost processability from the organic side.[11–13] Up to date, most organic-inorganic hybrid structured devices were demonstrated on rigid substrates,[10] since most inorganic materials typically need a rigid platform for their deposition or growth. Among inorganic materials used for photovoltaic or photo-sensing applications, Si nanowire seems to be one of the favorable materials due to their good electrical conductivity, wide spectrum of light absorption and good light harvesting capability.[12] However, the increasing demands for foldable or ultralight photovoltaic or photosensing applications require the development of higher performance flexible structures. To date, there are only very few reports describing flexible organic and inorganic hybrid structure. To realize mechanical flexibility in these hybrid structures, ZnO solution[13] or ZnO sol-gel[14] was used as electron transport layer or hole block layer. However, ZnO has innate limitation due to its wide bandgap, which is disadvantageous with regard to light absorption in the visible light spectrum.

The recent advances of releasable and transfer printable semiconductor nanomembranes (NMs), still inheriting the single crystal quality and the electronic properties of their bulk counterparts,[15–17] have enabled high performance inorganic semiconductors to be also applicable to flexible substrates.[18] In this paper, we describe the formation and properties of hetero p-n junctions formed between organic and inorganic materials, using specially designed n-type single crystal SiNM and p-type pentacene on a plastic substrate. Current-voltage, photoresponsivity, optical transmittance and mechanical bending properties were characterized for the flexible SiNM-pentacene p-n diodes.

J.-H. Seo, Prof. Z. Ma
Department of Electrical and Computer Engineering
University of Wisconsin-Madison
Madison, WI 53706, USA
E-mail: mazq@engr.wisc.edu
T.-Y. Oh, J. Park, Prof. B.-K. Ju
Display and Nanosystem Laboratory
College of Engineering
Korea University
Seoul, 136-713, Republic of Korea
E-mail: bkju@korea.ac.kr
Prof. W. Zhou
Department of Electrical Engineering
NanoFAB Center
University of Texas at Arlington
Arlington, TX 76019, USA

DOI: 10.1002/adfm.201203309

2. Results and Discussion

Figure 1 schematically illustrates the representative processing steps for fabricating the single crystalline SiNM and pentacene heterojunction diodes. The hexagonal shape corresponds to about 73% empty area of the total area of the released SiNM. The purpose of forming the hexagonal shape is to improve transparency and mechanical flexibility. The finished sample sitting on the PET substrates is bendable.

Figure 2a shows a microscopic image of the hexagonal SiNM that was transferred to a PET substrate. The left part of the SiNM is covered by Ti/Au metal. Figure 2b shows a zoom-in microscopic image of the SiNM. The right part of the SiNM is covered by a pentacene layer. The inset illustrates the device

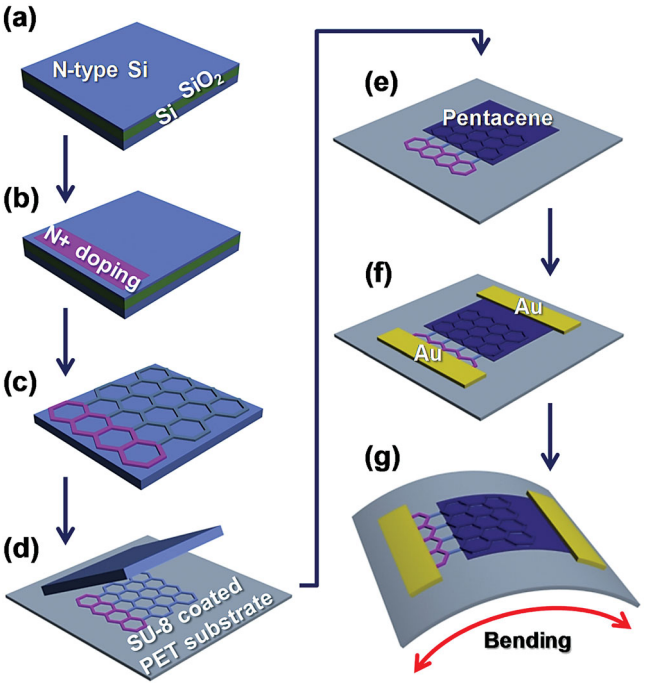

Figure 1. Schematic illustration of the fabrication process flow. a) Beginning with SOI (340 nm n-type top Si and 2000 nm buried oxide layer). b) N+ region was selectively doped to create an ohmic contact area using spin-on dopant. c) Patterning of active SiNM by RIE etching, followed by wet etching to undercut buried oxide layer. d) Transfer printing released SiNM to adhesive layer coated PET substrate with a PDMS stamp. e) Evaporation of pentacene on top of SiNM to form an organic-inorganic p-n junction. f) Metallization with e-beam metal evaporation to complete the fabrication process. g) The finished device is subject to bending.

cross sectional structure. Figure 2c shows a scanning electron microscopy (SEM) image of the SiNM-pentacene structure sitting on a PET substrate and the inset shows the cross-sectional illustration of the image. Figure 2d shows an atomic force microscopy (AFM) image of the deposited pentacene layer on top of the SiNM. The total device area is 1.82 cm^2 and the total non-empty area of the fabricated diode is 0.49 cm^2.

The measured forward and reverse bias *I–V* characteristics of the Si-pentacene heterojunction diode are shown in **Figure 3**a. The diode shows good rectifying behavior. To model the diode and also to plot the related band diagram between SiNM and pentacene, we express the *I–V* using the non-ideal diode equation, which includes the associated series resistance, based on the thermionic emission theory[19]

$$I = A_{\text{eff}} A^* T^2 \exp\left(\frac{-q\phi_B}{kT}\right) \exp\left(\frac{-q(V - IR)}{nkT}\right) \quad (1)$$

where V is the applied voltage, q is the electronic charge, n is the ideality factor, k is the Boltzmann constant, T is the temperature, R is the series resistance, A_{eff} is the active device area, A^* is the effective Richardson constant (112 A/cm^2 K^2 for n-type silicon) and φ_B is the barrier height.[20] At higher voltages, series resistance becomes dominant in the diode *I–V* characteristics. To analyze the series resistance effect, Equation (1) can be rearranged in terms of current density as[20,21]

$$V = RA_{\text{eff}} J + n\phi_B + \left(\frac{nkT}{q}\right) \ln\left(\frac{J}{A^{**}T^2}\right) \quad (2)$$

To calculate the series resistance and the ideality factor, Equation (2) can be differentiated with respect to the current density (J). By rearranging terms, we obtain d(V)/d(ln J) versus J plot.

$$\frac{d(V)}{d(\ln(J))} = RA_{\text{eff}} J + \frac{nkT}{q} \quad (3)$$

where R is the series resistance, n is the ideality factor. The barrier height of junction can be defined by an equation of current density[20,21]

$$F(J) = RA_{\text{eff}} J + n\phi_B \quad (4)$$

where φ_B is the barrier height.

By plotting d(V)/d(ln J) versus J, the series resistance R can be found from the slope and the ideality factor can be found from the y-axis intercept. The calculated series resistance R is 98 720 ohm and the ideality factor is found to be 1.94. This number is close to the ideality factor (n = 1.89) directly extracted from the measured *I–V* curve (Figure 1a, in dark). The electron barrier height of the diode was determined using the plot of $F(J)$ versus J and found to be 1.03 eV under equilibrium. Based on the calculation and other known parameters, the SiNM-pentacene band diagram is shown in Figure 3b. Based on Figure 3b, the barrier height encountered by holes is only 0.28 eV, much smaller than that encountered by electrons, under forward bias condition. Therefore, in this diode holes are the dominant transport charge carriers. Thus the overall diode characteristics, such as the forward current level, are largely decided by pentacene. Since pentacene is relatively an inefficient hole injector, we observed low current density (2.8 mA/cm^2) and high series resistance. The higher value of ideality factor may be also partially explained by the presence of native oxide on Si and/or possible degradation of pentacene layer.

The heterogeneous p-n diode was further characterized for photosensitivity. The results are also shown in Figure 3a. The measured dark current density is lower than 2×10^{-4} mA/cm^2 up to –5 V bias and is weakly dependent on the reverse-bias voltage. The photocurrent under the illumination of the three visible lasers (red: 633, yellow: 594 and green: 532 nm) were also shown for comparison with the dark current. The diode, biased at –5 V, exhibits a photocurrent of 2.8 mA/cm^2, 1.8 mA/cm^2 and 1.2 mA/cm^2 under the illumination of the red, yellow, and green lasers, respectively. The different photocurrent levels under different wavelengths may be ascribed to their penetration depths into SiNM. For the case of the 532 nm laser illumination, the ratio between the photo and the dark current is about 1.8×10^4 and the calculated photo responsivity is 0.7 A/W at –5 V. Apparently, this heterogeneous diode can be used as a flexible photodiode. The external quantum efficiency of the photodiode is calculated using $\eta_{EQE} = (I_{ph}/e)/(P_{in}/\hbar\nu)$, where I_{ph} is the photocurrent, P_{in} is the incident light power, and $\hbar\nu$ is the light energy. Figure 3c shows the η_{EQE} under the different wavelengths in the range from 473 nm to 905 nm. The highest η_{EQE} of 21.9% occurred at 632 nm. The drop of η_{EQE} at the shorter wavelengths is again presumably caused by their very shallow penetration depth. The SiNM is mainly responsible for the measured photosensitivity of the p-n diode, because it is known

Adv. Funct. Mater. **2013**,
DOI: 10.1002/adfm.201203309

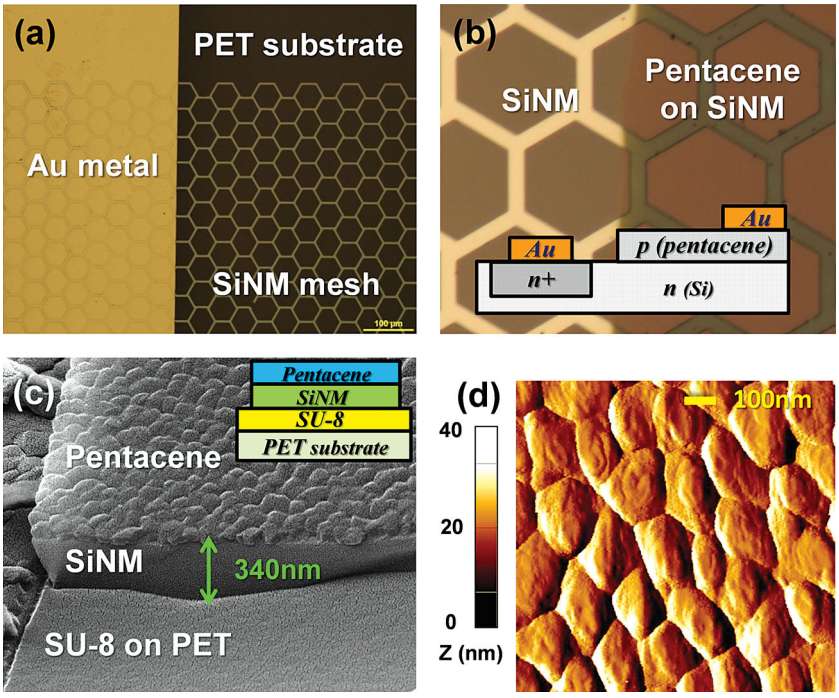

Figure 2. a) Microscopic image of transferred SiNM grid on PET substrate. b) Microscopic images of SiNM (left)/pentacene (right) heterojunction. The inset shows the cross section of the heterostructure. c) SEM image of SiNM and deposited pentacene layer sitting on SU-8 coated PET substrate. The inset shows the detailed layer structure. d) AFM image of deposited pentacene on Si NM. The average pentacene grain size is 180 nm.

that the optical absorption of pentacene layer is less than 10% in the most of visible wavelength range and only has relatively low absorption in the range of 600–700 nm.[9,27] However, compared to the device which has a similar structure (pentacene/n-type rigid Si) our device shows five times lower photoresponsivity.[28] The relatively low photo responsivity of the p-n diode is because the SiNM is very thin. Low photoresponsivity and η_{EQE} could be further improved by applying thicker SiNM or reflector layer on the plastic substrate.[29,30]

Both SiNM and pentacene are mechanically flexible. Applying these materials on flexible PET substrates make a flexible structure. The mechanical bending effects on the characteristics of the flexible diode were characterized. **Figure 4**a shows the *I–V* characteristics of the diode as a photodetector under shining of 633 nm light and different convex bending radii ranging from 77.5 mm to 15 mm. The calculated tensile strain due to bending ranges from 0.25% to 1.08% by the following equation: Strain(%) = $1/[(2R/\Delta R)+1]$, where R is the fixture radius, ΔR is the thickness of the bended object. ΔR includes the thickness of PET substrate, SU-8 layer, SiNM, and pentacene layer. Figure 4b plots the photocurrent change (at –5 V bias) as a function of the bending strain. Before bending, the external quantum efficiency is 21.9% and the photoresponsivity was 0.7 A/W at –5 V. Under bending with the application of 1.08% strain, the photocurrent at –5 V bias slightly increases from 2.8 mA/cm^2 to 3.3 mA/cm^2. The corresponding external quantum efficiency and photoresponsivity increase to 25.1% and 1.08 mA/W, respectively, at the same bias. Figure 4c show the overall diode image under bent condition.

To understand the performance change of the photosensitive diode during bending, a Horiba LabRAM ARAMIS Raman confocal microscope was used to examine the strain status of the diode materials. A 50× objective was used to focus 18.5 mW of He-Ne (632.8 nm) laser light onto the sample surface with a spot size of about 1 μm and spectrometer resolution of 0.045 cm^{-1}. With this spot size, the actual laser power directed to the sample is ≈6.9 mW. **Figure 5** shows the Raman spectrum of the pentacene and SiNM without and with bending (1.08% tensile strain). The Raman peaks at 1158 and 1178 cm^{-1} originate from the C-H in plane vibration and the peaks at 1340 and 1390 cm^{-1} (not shown) originate from the C-C aromatic stretching vibration. The C-C peaks indicate the intermolecular interactions, while C-H interaction is the evidence of the in-phase and out-of-phase intermolecular coupling. Therefore, by observing the C-H interaction under bending conditions, the molecules' coupling status can be inspected. Before applying bending, three peaks, which indicate the vibration modes of pentacene, at 1155.2 cm^{-1} (ν_1), 1157.0 cm^{-1} (ν_0), and 1162.0 cm^{-1} (ν_2) can be de-convoluted using the Gaussian/Lorentzian function in the wave number range of 1140 cm^{-1} to 1170 cm^{-1}. Under the bending (1.08% tensile strain) condition, the ν_0 peak shifts from 1157.0 cm^{-1} to 1158.4 cm^{-1}, while the ν_1 and ν_2 peaks remain similar to 1155.3 cm^{-1} and 1162.3 cm^{-1}, respectively. The shift of the ν_0 peak indicates that pentacene is under stretching due to the tensile strain applied. The Si Raman peak shifts from 522.1 cm^{-1} to 519.7 cm^{-1} under the bending condition, also indicating the tensile strain being applied to the SiNM. Previous study showed that the difference between ν_0 and ν_1 ($\Delta\omega$) is highly related to mobility improvement of pentacene layer.[22,23] We therefore expect that the strain applied to pentacene has improved the pentacene mobility. It is also known that uniaxial tensile strain of Si enhances both electron and hole mobility of SiNMs by the deformation of crystal lattice.[24–26] Therefore, the observed photocurrent increase under bending can be explained on the basis of hole mobility increase in both Si and pentacene.

The mesh structure design of the thin SiNM along with pentacene is expected to provide high optical transparency of the heterogeneous diode structure. The transmittance spectrum of the diode sample including its 250 μm PET substrate and the adhesive SU-8 layer is shown in **Figure 6**a, along with the spectra of PET only, PET/SU-8 and Pentacene/SU-8/PET for comparison. With such multiple layers that consists of a 250 μm thick PET, an average transmittance of 63% in the visible range (400–750 nm) was still measured. Using the same configuration, but without the SiNM layer, an average transmittance of 69% in the visible range was observed. The small degradation of transmittance with the presence of the SiNM is ascribed to the patterned hollow hexagonal structure in the

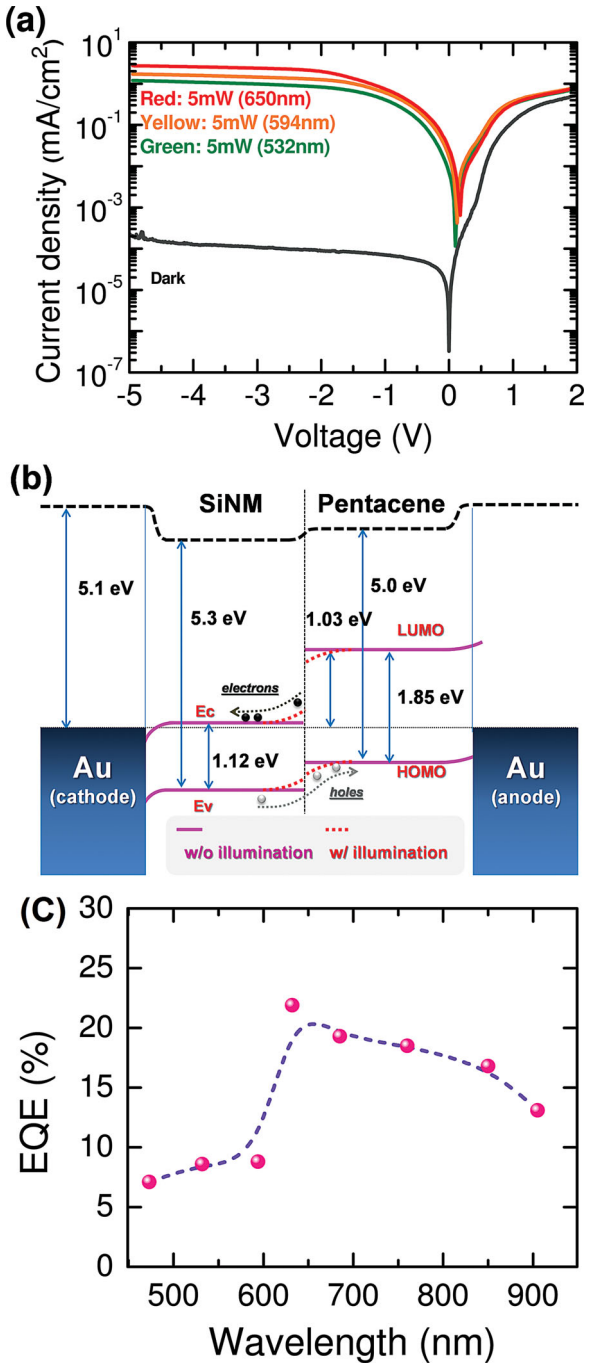

Figure 3. a) Current-voltage characteristics of the diode in dark and under illumination of lasers with wavelengths of 532, 594, and 633 nm, respectively. The laser light intensity is 5 mW. b) Calculated band diagram of SiNM-pentacene heterojunction. c) η_{EQE} spectrum as a function of various wavelengths from 473 nm to 905 nm. The line is to aid the view of the figure.

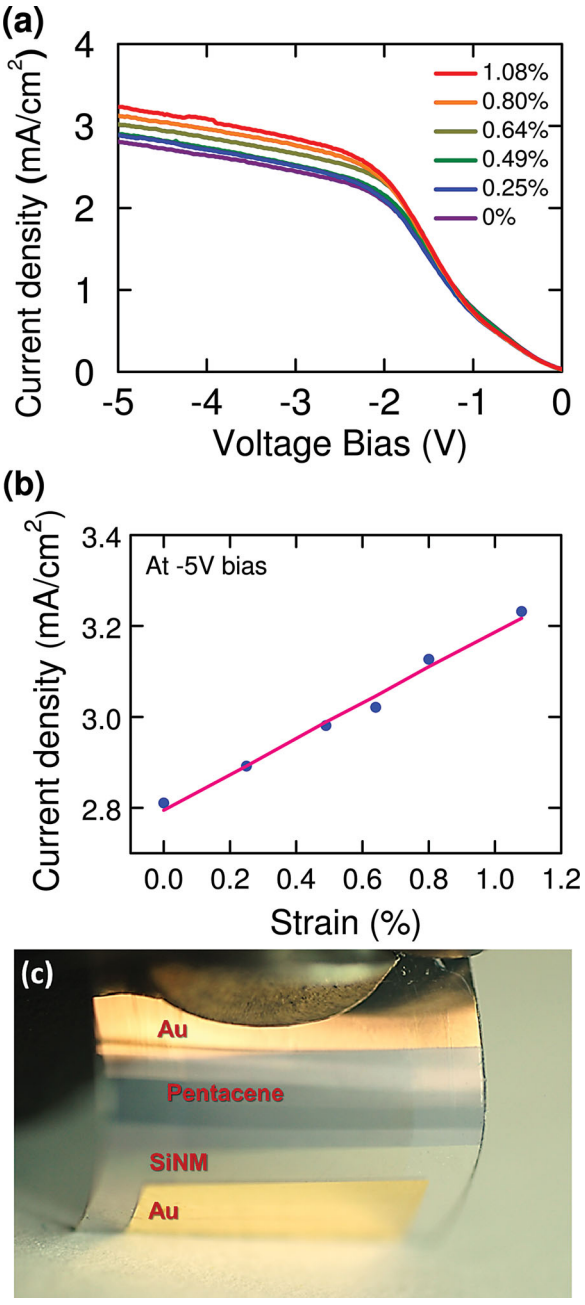

Figure 4. Characterizations SiNM-pentacene diode under mechanical bending. a) Measured photocurrent of the diode under different bending strain. b) Plot of photocurrent change as a function of strain. c) An optical image of the diode under bending.

SiNM, besides its thinness. Evidently, the SiNM-pentacene heterostructure itself displays high transparency. An optical image of the diode sample exhibiting transparency is shown in Figure 6b. Combined with the displayed features of the SiNM-pentacene diode, including the rectification, the photo sensitivity, the bendability and the transparency, the heterogeneous organic-inorganic p-n junction diode could be used for many functional devices.

3. Conclusion

We demonstrated a multifunction organic-inorganic heterogeneous p-n junction by complementally combining flexible single-crystal n-type silicon nanomembrane and p-type

Adv. Funct. Mater. **2013**,
DOI: 10.1002/adfm.201203309

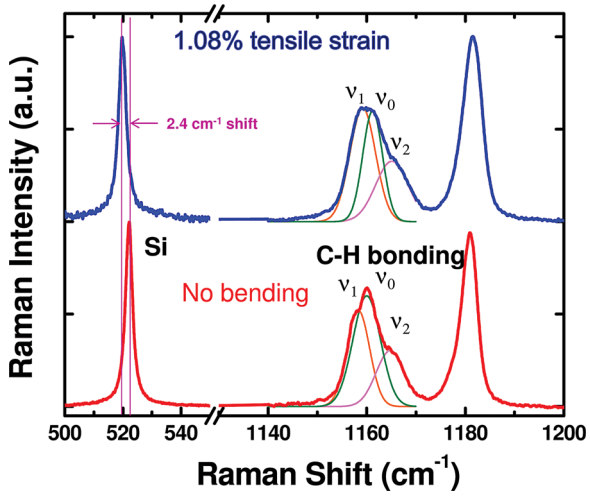

Figure 5. Raman spectra of the SiNM-pentacene diode without and with bending. The Gaussian/Lorentzian functions used for the de-convolution of overlapped Raman peaks. C-H in plane vibration is displayed at the peaks of 1158 and 1178 cm^{-1}. Under bending (tensile strain applied), the ν_0 band shifts from 1157.0 cm^{-1} to 1158.4 cm^{-1} and the Si peaks shifts from 522.1 cm^{-1} to 519.7 cm^{-1}.

pentacene layer on a plastic substrate. The heterostructure exhibits mechanical flexibility, optical transparency, rectifying and photosensitive characteristics. The successful functional integration between organic and special form inorganic materials suggests that such heterogeneous integration approach could be a viable strategy to fabricate flexible organic and inorganic hybrid devices. Although we used pentacene as an example in this work, other polymer semiconductor materials may also be applied.

4. Experimental Section

Device Fabrication: The fabrication began with a silicon-on-insulator (SOI) wafer (Soitec Unibond with a n-type 340 nm top Si layer with doping level of 1.0–4.0 × 10^{15}/cm^3) (Figure 1a). Heavily doped regions were formed on the template layer for an ohmic contact via phosphorous diffusion using a spin-on-dopant (P509, Filmtronics, USA). The drive-in diffusion process was carried out at 800 °C by rapid thermal annealing for 30 min (Figure 1b). After finishing photolithography and reactive ion etching (RIE) steps for defining the hexagonal mesh on the top of Si template layer, the 2 µm buried oxide layer of the SOI was undercut with concentrated (49%) hydrofluoric acid. The released top Si layer forms SiNM, which mechanically very flexible, and is ready to be transferred to a foreign substrate (Figure 1c). By utilizing an elastomeric polydimethylsiloxane (PDMS) stamp, the released SiNM was picked up and transferred to a 250 µm thick polyethylene terephthalate (PET) substrate that was pre-coated with 1.5 µm SU-8 as an adhesives layer (SU-8 2002, Microchem) (Figure 1d). On top of the transferred SiNM, 70 nm thick pentacene thin film was thermally evaporated with a deposition rate of 0.3 Å/s (Figure 1e), followed by metal evaporation of Ti/Au of 5 nm/350 nm for electrodes (Figure 1f). The finished sample sitting on the PET substrates is bendable (Figure 1g).

Device Characterization: The *I–V* characteristics were measured using a semiconductor parameter analyzer (HP4155B) in the dark to avoid any light induced photocurrents. The photosensitivity of the organic-inorganic heterojunction photodetector was characterized using different laser wavelengths (λ) (473, 532, 594, 632, 685, 760, 850, and 905 nm), all at a power intensity of 5 mW. The laser beam spot diameter is 800 µm and the laser shining area is 0.005 cm^2. The non-empty (effective) area receiving laser light is 0.00135 cm^2.

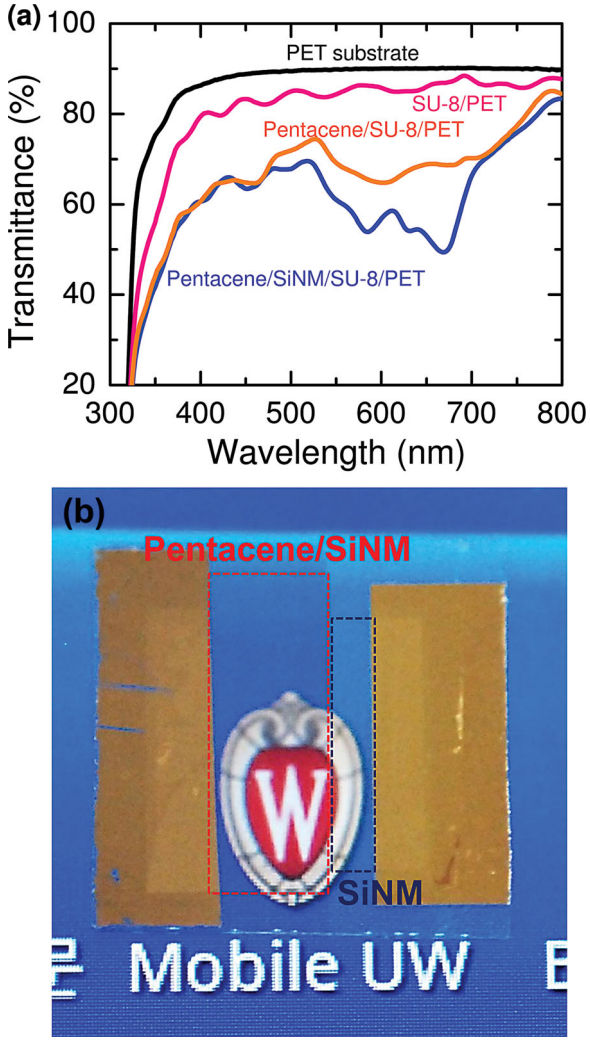

Figure 6. a) The transmittance spectra of a bare PET substrate, PET coated with SU-8, pentacene on SU-8 coated PET and the final device structure consisting of pentacene/SiNM/SU-8/PET. b) An optical image of the sample showing its transparency.

Acknowledgements

J.-H.S. and T.-Y.O. contributed equally to this work. The work is supported by AFOSR, under grants FA9550-091-0482 and FA9550-08-1-0337, and supported by Basic Science Research Program through the National Research Foundation of Korea (NRF) funded by the Ministry of Education, Science and Technology (2012R1A6A3A04039396), and the RFID R&D program of MKE/KEIT (10035225, Development of core technology for high performance AMOLED on plastic). The program manager at AFOSR is Dr. Gernot Pomrenke.

Received: November 12, 2012
Revised: January 8, 2013
Published online:

[1] M. J. Sailor, E. J. Ginsburg, C. B. Gorman, A. Kumar, R. H. Grubbs, N. S. Lewis, *Science* **1990**, *249*, 1146.
[2] C. Chen, I. Shih, *J. Mater. Sci. Mater.* **2006**, *17*, 1047.
[3] M. C. Scharber, D. Mühlbacher, M. Koppe, P. Denk, C. Waldauf, A. J. Heeger, C. J. Brabec, *Adv. Mater.* **2006**, *18*, 789.
[4] Y. Matsumoto, J. C. Nolasco, *PVSC '08. 33rd IEEE* **2008**, San Diego, CA, USA, 1.
[5] S. H. Park, A. Roy, S. Beaupre, S. Cho, N. Coates, J. S. Moon, D. Moses, M. Leclerc, K. Lee, A. J. Heeger, *Nat. Photonics* **2009**, *3*, 297.
[6] T. Ameri, G. Dennler, C. Waldauf, H. Azimi, A. Seemann, K. Forberich, J. Hauch, M. Scharber, K. Hingerl, C. J. Brabec, *Adv. Funct. Mater.* **2010**, *20*, 1592.
[7] L. Wang, D. Zhao, Z. Su, F. Fang, B. Li, Z. Zhang, D. Shen, X. Wang, *Org. Electron.* **2010**, *11*, 1318.
[8] A. Tada, Y. Geng, Q. Wei, K. Hashimoto, K. Tajima, *Nat. Mater.* **2011**, *10*, 450.
[9] S. Avasthi, S. Lee, Y.-L. Loo, J. C. Sturm, *Adv. Mater.* **2011**, *23*, 5762.
[10] F. Zhang, X. Xu, W. Tang, J. Zhang, Z. Zhuo, J. Wang, J. Wang, Z. Xu, Y. Wang, *Sol. Energy Mater. Sol. Cells* **2011**, *95*, 1785.
[11] S. R. Forrest, M. L. Kaplan, P. H. Schmidt, *J. Appl. Phys.* **1984**, *55*, 1492.
[12] F. Zhang, X. Han, S.-T. Lee, B. Sun, *J. Mater. Chem.* **2012**, *22*, 5362.
[13] F. C. Krebs, M. Jørgensen, K. Norrman, O. Hagemann, J. Alstrup, T. D. Nielsen, J. Fyenbo, K. Larsen, J. Kristensen, *Sol. Energy Mater. Sol. Cells* **2009**, *93*, 422.
[14] H.-J. Park, K.-H. Lee, B. Kumar, K.-S. Shin, S.-W. Jeong, S.-W. Kim, *J. Nanoelectron. Optoelectron.* **2010**, *5*, 135.
[15] L. Sun, G. Qin, J.-H. Seo, G. K. Celler, W. Zhou, Z. Ma, *Small* **2010**, *6*, 2473.
[16] J. Yoon, A. J. Baca, S.-I. Park, P. Elvikis, J. B. Geddes, L. Li, R. H. Kim, J. Xiao, S. Wang, T.-H. Kim, M. J. Motala, B. Y. Ahn, E. B. Duoss, J. A. Lewis, R. G. Nuzzo, P. M. Ferreira, Y. Huang, A. Rockett, J. A. Rogers, *Nat. Mater.* **2008**, *7*, 907.
[17] H. Yang, D. Zhao, S. Chuwongin, J.-H. Seo, W. Yang, Y. Shuai, J. Berggren, M. Hammar, Z. Ma, W. Zhou, *Nat. Photonics* **2012**, *6*, 615.
[18] K. Zhang, J.-H. Seo, W. Zhou, Z. Ma, *J. Phys. D: Appl. Phys.* **2012**, *45*, 143001.
[19] S. M. Sze, *Physics of Semicondutor Devices 2nd ed.*, Wiley, New York **1981**.
[20] S. K. Cheung, N. W. Cheung, *Appl. Phys. Lett.* **1986**, *49*, 85.
[21] J. H. Werner, H. H. Guttler, *J. Appl. Phys.* **1993**, *73*, 1315.
[22] H. L. Cheng, X. W. Liang, W. Y. Chou, Y. S. Mai, C. Y. Yang, L. R. Chang, F. C. Tang, *Org. Electron.* **2009**, *10*, 289.
[23] H. L. Cheng, W. Y. Chou, C. W. Kuo, F. C. Tang, Y. W. Wang, *Appl. Phys. Lett.* **2006**, *88*, 161918.
[24] A. S. Shelley, G. L. Max, *J. Phys. D: Appl. Phys.* **2007**, *40*, R75.
[25] C. Feng, E. Chanan, L. Zheng, F. J. Himpsel, L. Feng, G. L. Max, *J. Phys. D: Appl. Phys.* **2011**, *44*, 325107.
[26] C. Y. Peng, C. F. Huang, Y. C. Fu, Y. H. Yang, C. Y. Lai, S. T. Chang, C. W. Liu, *J. Appl. Phys.* **2009**, *105*, 083537.
[27] I. H. Campbell, B. K. Crone, *J. Appl. Phys.* **2009**, *106*, 113704.
[28] S. Kim, S. Park, J. Kim, S. Im, *Thin Solid Films* **2002**, *420*, 19.
[29] A. Polzer, W. Gaberl, H. Zimmermann, *Electron Lett.* **2011**, *47*, 614.
[30] J. C. Shin, M. K. Parsian, J. Y. Ki, T. Stephanie, M. H. Kyle, M. L. Lee, J. A. Rogers, X. Li, *ACS Nano* **2012**, *6*, 11074.

Adv. Funct. Mater. **2013**,
DOI: 10.1002/adfm.201203309